Journal of Membrane Science 624 (2021) 119122

Contents lists available at ScienceDirect

Journal of Membrane Science

journal homepage: http://www.elsevier.com/locate/memsci

Secondary growth of bi-layered covalent organic framework nanofilms with offset channels for desalination

Ankang Xiao, Xiansong Shi **, Zhe Zhang, Congcong Yin, Sen Xiong, Yong Wang *

State Key Laboratory of Materials-Oriented Chemical Engineering, College of Chemical Engineering, Nanjing Tech University, Nanjing, 211816, Jiangsu, PR China

ARTICLE INFO

Keywords:
Covalent organic frameworks
Secondary growth
Offset channels
Narrowed effective aperture
Desalination

ABSTRACT

Processing two-dimensional (2D) covalent organic frameworks (COFs) into nanofilms has gained widespread attention in water treatment. However, the designed synthesis of COF-based membranes for ion separations still remains a huge challenge though the strategies to produce COF molecular separation membranes have been greatly developed. Herein, we report the construction of bi-layered COF nanofilms for efficient desalination through a simple yet effective secondary growth. The suggested strategy is capable of easily regulating the growth of another COF layer on the pre-synthesized first layer, thus producing crystalline and defect-free bi-layered COF nanofilms with distinct laminated structures. Most importantly, the offset channels are involved at the interface of two nanofilms obtained from the first and secondary growth, which leads to a constricted effective aperture that significantly enhances the ion separation performance. Specifically, the bi-layered COF nanofilms composited with macroporous supports exhibit high rejection rates (~95.8%) to Na_2SO_4, observably surpassing the desalination performance of single-layered COF nanofilms (rejection<10%). This work not only develops an ingenious way to fabricate COF-on-COF nanofilms with narrowed channels by tailoring the laminated structure of 2D COFs at the film interface, but also starts an avenue for the adoption of COF platforms for membrane separations with an improved precision.

1. Introduction

Covalent organic frameworks (COFs), constructed from periodic organic building blocks, are a novel kind of porous crystalline polymers with regular channels, permanent porosity, excellent stability, high surface areas and readily-tailored functionalities [1,2]. These merits of COFs based on various building blocks and topological structures can satisfy different requirements in extensive areas, including gas storage [3,4], catalysis [5,6], photoelectricity [7,8], separation [9,10], and etc. [11,12] In particular, the ordered channels and excellent stability of COFs enable them as promising candidates for the preparation of high-performance separation membranes with ultra-high permselectivity [10]. Compared with traditional amorphous polymers, the well-defined in-plane pores and high porosity endow COF-based membranes with high separation precision and fast water permeation [9,13].

Currently, a number of COF membranes have been fabricated by various methods including *in-situ* growth [14–16], interfacial synthesis [17–19], COF nanosheets assembly [20–22], and etc. [23–26] Particularly, *in-situ* growth under solvothermal process plays an important role in assembling COF microcrystals into well-aligned membrane architectures, which can promote crystallization of COFs and cause "self-healing", and lead to highly crystalline COF separation layers. Up to now, considerable efforts have been made to produce COF-based membranes by the *in-situ* growth method in solvothermal process. For instance, by adopting this preparation strategy Caro and co-workers prepared COF-LZU1 membranes with a thickness of ~400 nm on modified alumina ceramic tubes, realizing high permeation fluxes and effective rejections to various dyes [27]. Previously, we directly utilized solvothermal synthesis to grow COFs on anodic aluminum oxide (AAO) substrates with sharp variation of selectivity from ultrafiltration to nanofiltration [28]. Moreover, we also reported a new polymer-assisted transfer method to produce COF membranes with good separation capability to various dyes [29]. In general, the pore size of most COFs above is in the range of 0.84 nm–5.1 nm [30]. By virtue of the design and tailor-made function of pore sizes, these COFs based membranes have achieved the effective sieving of small molecules. Since the hydrated ion diameter of inorganic salt ions (monovalent and bivalent salts) is smaller than the inherent-pore size of COFs, these COF based membranes failed

* Corresponding author.
** Corresponding author.
E-mail addresses: xiansong_shi@njtech.edu.cn (X. Shi), yongwang@njtech.edu.cn (Y. Wang).

https://doi.org/10.1016/j.memsci.2021.119122
Received 15 November 2020; Received in revised form 31 December 2020; Accepted 26 January 2021
Available online 2 February 2021

to exhibit pronounced rejections to salt ions, and it is still very limited for ion separations.

It should be noted that some attempts have been made to prepare COF based membranes with reduced pore sizes for ion separations. Huang and co-workers reported a COF membrane with high salt ion rejection (96.3% for Na_2SO_4) and relatively fast permeances (0.5 L m^{-2} h^{-1} bar^{-1}) through post-synthetic modification [31]. The post-synthetic modification can enable COF membranes constricted pore apertures, but the process is usually complicated and tedious. Alternatively, Ma and co-workers employed a modified interfacial polymerization method to grow a free-standing COF membrane and the stacking mode of 2D COF layers themselves can be adjusted from AA stacking to AB stacking by using different precursors. The obtained AB stacking COF membrane with narrow aperture (~0.6 nm) showed Na_2SO_4 or K_2SO_4 rejection values between 90 and 95% [32]. We also studied the performance of offset-eclipsed COF layers themselves in desalination by molecular dynamics simulations, and the permeability of COF membranes decreased with rising stacking number of COF multilayers [33]. Unfortunately, the formation of offset-eclipsed 2D COF layer itself is hard to control in the experimental procedure. As a result, the development of a simple strategy to COF membranes for desalination still remains a formidable challenge.

Recently, Caro and co-workers have prepared COF-LZU1−ACOF-1 bilayer membranes with interlaced pore networks for selective gas separation [34]. Inspired by this work, we believe that the offset channels at the interface of two nanofilms can be easily realized compared with offset-eclipsed COF layers themselves via the *in-situ* growth method. Therefore, the solvothermal growth can be employed to obtain well-defined and crystalline COF nanofilms and construct offset channels at the interface between two nanofilms inherited from the first and secondary growth, which exerts facile control over the microstructure and thickness, and is expected to enable desired separation performance in desalination.

In this work, we select the azine-linked ACOF-1 with sub-nanopores of 0.94 nm to engineer the bi-layered separation nanofilms for desalination through a secondary growth method. Dense and tunable bi-layered ACOF-1 nanofilms are obtained after secondary growth to produce constricted pore sizes. The bi-layered ACOF-1 nanofilms can be transferred from silicon wafers onto porous substrates without any defects by the perforated polymer-assisted transfer method [29]. The prepared ACOF-1 composite membranes exhibited reasonable fluxes and high rejection rates toward Na_2SO_4. The secondary growth method reported in this work demonstrates a novel protocol under solvothermal conditions to prepare bi-layered COF nanofilms with narrowed pores between two adjacent COF nanofilms for effective rejection of salt ions, which is expected to open up the application of COFs in desalination.

2. Experimental

2.1. Materials

All chemicals were used herein without further purification. 1,3,5-triformylbenzene (TFB, 95%) was obtained from Jilin Yanshen Technology Co., Ltd., China. Hydrazine hydrate ($Hz{\cdot}H_2O$, 98%) was purchased from Aladdin. The polysulfone-*block*-poly(ethylene glycol) (PSF-*b*-PEG) block copolymer was purchased from Nanjing Bangding, and the PEG block was 21 wt% of a total molecular weight of 79.1 kDa. Silicon wafers with a top layer of silicon dioxide (~1000 nm in thickness) were served as smooth substrates for the growth of COF nanofilms. Poly(ether sulfone) (PES) membranes with a nominal pore diameter of ~0.22 μm (ø = 2.5 cm, Jin Teng) were served as the substrate to support the transferred bi-layered COF nanofilms. Polyethylene glycols (PEGs, M_w=200 Da, 400 Da, 600 Da, 1000 Da, 2000 Da) were obtained from Aladdin. 1,4-dioxane (99.0%), chloroform (99.5%), acetone (99.5%), ethanol (99.5%), acetic acid (AA, 99.5%), hydrofluoric acid (HF, 40.0%) and inorganic salts (99.0%) were supplied by local suppliers. Deionized (DI) water (conductivity: 2–5 μS cm^{-1}, Wahaha) was used throughout this work.

2.2. Synthesis of ACOF-1 nanofilms

ACOF-1 nanofilms were prepared on silicon wafers via a two-step solvothermal synthesis strategy (Scheme 1). In the first growth, TFB (0.096 mmol, 15.6 mg) was dissolved in 20 mL of 1, 4-dioxane and formed the concentration of 4.8 mmol L^{-1} (mM). Hz (20 μL) was then added and the mixture was sonicated for 15 min to obtain a homogenous solution. Subsequently, three silicon wafers faced downwards were placed into a 3D-printed nylon shelf with three parallel slots, adding AA (500 μL) as the catalyst. Afterwards, a Teflon-lined stainless-steel autoclave was used to hold the nylon shelf and heated at 120 °C in an oven. After reaction for 12 h, the autoclave was cooled down to room temperature, and ACOF-1 layers grown on silicon wafers were washed with 1, 4-dioxane and ethanol for several times to remove the residual powders. Finally, the single-layered ACOF-1 nanofilms were dried at 90 °C overnight. In addition, ACOF-1 nanofilms with increased thicknesses were also obtained under the TFB concentration of 9.6 mM and reaction time of 36 h.

The process for the secondary growth was the same as above, whereas the TFB concentrations for the synthesis were varied from 1.2 mM to 14.4 mM with the corresponding Hz amount under same volume of solvent. After secondary growth for various durations from 6 h to 48 h, the silicon wafers grown with bi-layered ACOF-1 nanofilms were taken out and thoroughly washed with 1, 4-dioxane and ethanol. ACOF-1 powders were also collected from the bottom product of free solution after the growth of ACOF-1 nanofilms, followed by drying at 120 °C for 24 h.

2.3. Preparation of ACOF-1 composite membranes

ACOF-1 composite membranes were prepared through a previously reported procedure [29], and the detailed fabrication process is shown in Fig. S1. Firstly, the PSF-*b*-PEG layer was constructed on the top of bi-layered ACOF-1 nanofilms by spin coating its dilute solution (2000 rpm, 30 s). The resulting samples were left into two-component solvent containing 80 wt% of ethanol and 20 wt% of acetone at 70 °C for 1 h and then dried at room temperature. 5 wt% HF aqueous solution was then adopted to etch away the silicon dioxide layer, thus releasing the BCP-coated ACOF-1 nanofilms. The BCP-coated ACOF-1 nanofilms were then transferred onto DI water and composited with macroporous PES supports to form composite membranes.

2.4. Characterizations

Fourier transform infrared (FTIR) spectra of ACOF-1 monomers, powders, and nanofilms were recorded by an infrared spectroscopy (Nicolet 8700). Powder X-ray diffraction (PXRD) patterns of ACOF-1 powders and nanofilms were acquired on a diffractometer (Rigaku, SmartLab) with a scan speed of 0.02° s^{-1} in 2θ angles from 2° to 40°. The thickness of ACOF-1 nanofilms on silicon wafers were obtained by a spectroscopic ellipsometry (Complete EASEM-2000U, J. A. Woollam) at an incidence angle of 70° with the wavelength ranging from 400 nm to 999.8 nm. Scanning electron microscopy (SEM, Hitachi S-4800) was used to observe the surface and cross-sectional morphologies of samples at an accelerating voltage of 5 kV, and all samples were sputter-coated with a thin layer of gold before SEM characterizations. An atomic force microscope (AFM, XE-100, Park systems) was used to observe the three-dimensional morphology of the membrane surface and conducted at a noncontact mode. Transmission electron microscope (TEM) was conducted on a Tecnai 12 microscope (Philips Company, Holland) operated at 200 kV after transferring ACOF-1 nanofilms onto carbon-coated copper grids. Nitrogen adsorption-desorption measurements of ACOF-1 powders prepared by the first and secondary growth were

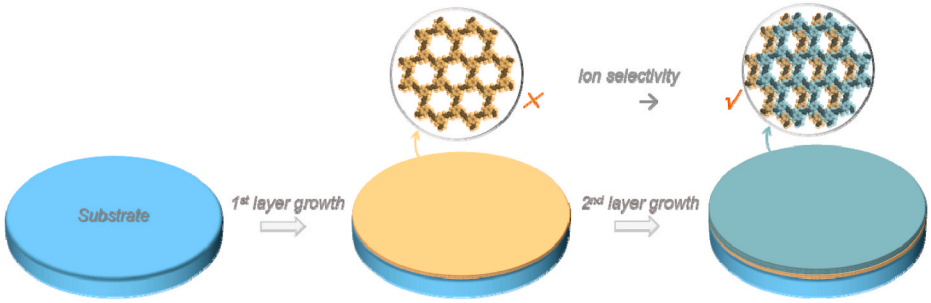

Scheme 1. Schematic illustration for the growth of ACOF-1 nanofilms.

conducted via the Micrometrics ASAP 2460 surface area and porosity analyzer at 77 K, and the pore size distributions were obtained from the sorption curves based on the nonlocal density functional theory (NLDFT). The water contact angle (WCA) measurements of ACOF-1 nanofilms on silicon wafers were performed on a contact angle goniometer (DropMeter A100, Maist) with three different positions. The concentrations of various inorganic salts were recorded by an electrical conductivity meter (S230–K, Mettler-Toledo). The concentrations of various PEGs were measured by a gel permeation chromatography (GPC, Waters 1515).

2.5. Desalination performance evaluation

A dead-end filtration system (Amicon 8003, Millipore) was employed to evaluate the fluxes and rejection rates of the prepared ACOF-1 composite membranes. ACOF-1 composite membranes were tested under a pressure of 3 bar with a stirring rate of 500 rpm to avoid the concentration polarization. Various inorganic salts including Na_2SO_4, $MgSO_4$, $MgCl_2$, and NaCl, with a concentration of 1000 ppm, were used as feed solutions for rejection tests. The flux of ACOF-1 composite membranes was calculated by the following equation.

$$F=V/S\,t \quad (1)$$

where F is the flux of solution (L m^{-2} h^{-1}), V represents the volume of permeated salt feed solutions (L), t is permeated time (h) across the membrane, and S is effective membrane area (m^2).

The salt rejection rates of ACOF-1 composite membranes were calculated by the following equation.

$$R = (1- C_p/C_f) \times 100\% \quad (2)$$

where R is inorganic salt rejection rate (%), C_p are the concentration (ppm) of the salt permeation and C_f is the concentration of salt feed. In all the filtration tests of ACOF-1 composite membrane, more than three membranes were recorded to obtain average values.

Molecular weight cutoff (MWCO) and pore size distribution were obtained according to the rejection of PEGs with various molecular weights (200 Da, 400 Da, 600 Da, 1000 Da, and 2000 Da). Each PEG is dissolved in water to form a concentration of 750 ppm. To avoid the concentration polarization, ACOF-1 composite membranes were also tested under a vigorous stirring rate of 500 rpm. The Stokes radius of PEG was calculated by the following equation:

$$r_p=16.73 \times 10^{-12} \times M_w^{0.557} \quad (3)$$

where r_p represents the Stokes radius (m), and M_w is its average molecular weight.

The pore size distribution can be obtained from probability density function and the Stokes radius [35].

3. Results and discussion

3.1. Structural characterizations of ACOF-1 nanofilms

To satisfy the desalination performance, ACOF-1 nanofilms, constructed by short hydrazine and aldehyde to form azine-linked frameworks that possess desired stability and sub-nanometer vertical channels (Fig. 1a), are grown on silicon wafers under solvothermal synthesis. The offset channels at the interface of two nanofilms can be achieved after secondary growth. As shown in Fig. S2, with the first growth of single-layered ACOF-1 nanofilms the initially undefiled silicon wafer turns violet, which becomes darker after the secondary growth. The homogeneous color on the substrate after each growth evidences that the COF layer is uniformly deposited on the silicon substrate. The successful synthesis of ACOF-1 nanofilms and powders was then confirmed by FTIR (Fig. 1b). The spectra of ACOF-1 nanofilms and powders both exhibit obvious C═N stretching vibration peaks at 1623 cm^{-1}, indicating the occurrence of condensation reaction to form azine-linked frameworks. Compared with the monomer TFB, the disappearance of C═O stretching vibration peaks at 1695 cm^{-1} and C–H stretching vibration peaks at 2892 cm^{-1} assigned to the aldehyde proves a complete consumption of building blocks [36,37]. For precise ion separations, the regularity of pore sizes is considered as an important factor that could directly determine the sieving performance. Here, the ordered structure of synthesized ACOF-1 nanofilms and powder counterparts was determined by the PXRD characterization, as given in Fig. 1c. Clearly, the powders produced during the nanofilm synthesis exhibit a satisfied crystallinity, which show an intense peak at around ~7° that can be assigned to the (100) crystal plane. Besides, the presence of a relatively broad peak at $2\theta = 27°$ is mainly due to the π-π stacking between the stacked ACOF-1 layers, corresponding to the (001) plane [15,34]. Given the same synthesis condition, the crystallinity of the powders recorded here is eligible to reflect the ordered pore structure of the nanofilm, which is further demonstrated by the nanofilm PXRD result. Moreover, the PXRD diffraction peaks of ACOF-1 nanofilms are relatively weak, which could be mainly attributed to the ultra-thin thickness of the naofilm.

3.2. Investigation on the growth of ACOF-1 nanofilms

The preparation of bi-layered ACOF-1 nanofilms greatly depends on both the first growth and the secondary growth during the solvothermal process. Single-layered ACOF-1 nanofilms were firstly grown on the surface of the silicon wafer, and the terminal amino and aldehyde groups on the nanofilm surface can provide a large number of nucleation sites, promoting the secondary growth of single-layered ACOF-1 nanofilms. The secondary growth is expected to enable two adjacent ACOF-1 nanofilms offset against each other at the interface and form interlaced pores, which contributes to the production of bi-layered ACOF-1 nanofilms with narrowed pore sizes that are available for ion separations.

In this work, the first growth of single-layered ACOF-1 is very important, and therefore the different concentrations of the first growth

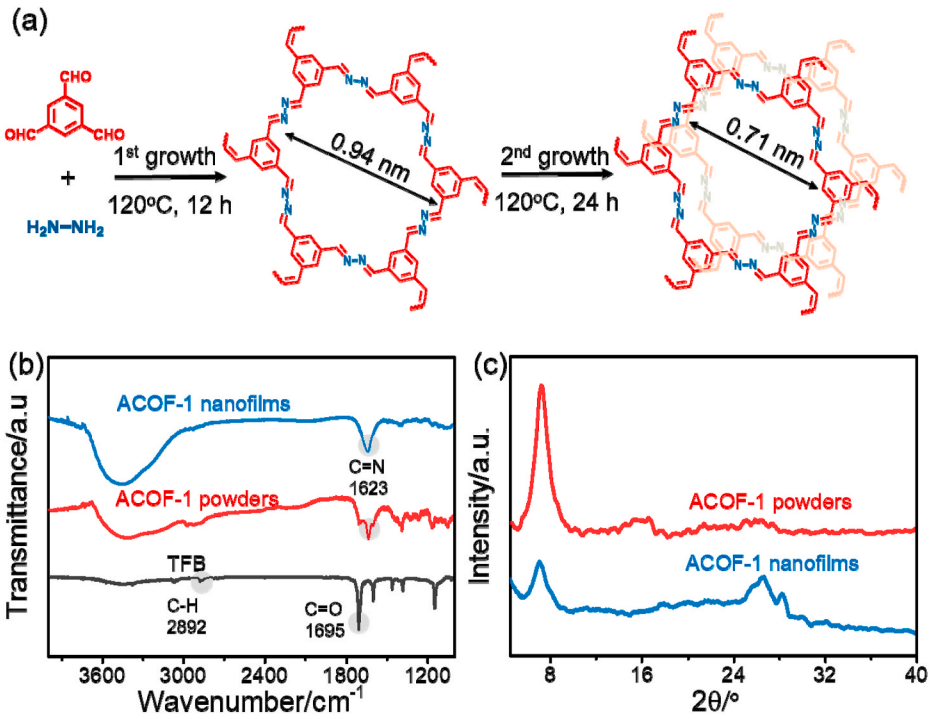

Fig. 1. Structural characterizations of ACOF-1 nanofilms synthesized by the Schiff-base reaction. (a) Reaction scheme of TFB and Hz to form ACOF-1 structure after first growth and secondary growth. (b) FTIR spectra of TFB, ACOF-1 powders and nanofilms. (c) PXRD patterns of ACOF-1 powders and nanofilms.

were adequately investigated to obtain continuous ACOF-1 first layers. In order to avoid thicker nanofilms, we studied the growth of ACOF-1 on the surface of silicon wafers at reasonable reaction time of 12 h. At lower TFB concentration of 1.2 mM, only some disordered ACOF-1 microcrystals appear on the silicon wafers due to the insufficient growth of nanofilms (Fig. 2a). When the TFB concentration increases to 2.4 mM, massive ACOF-1 microcrystals gradually grow into small domains, but these domains seem to be separated by large gaps from each other (Fig. 2b). As TFB concentration increases to 4.8 mM, a continuous ACOF-1 nanofilm forms on the surface of silicon wafer (Fig. 2c), indicating that increased TFB concentrations can promote a complete grain intergrowth. Based on the microscopic observation, the first growth under solvothermal conditions is optimized with reaction time of 12 h and TFB concentration of 4.8 mM. After the first growth, the single-layered

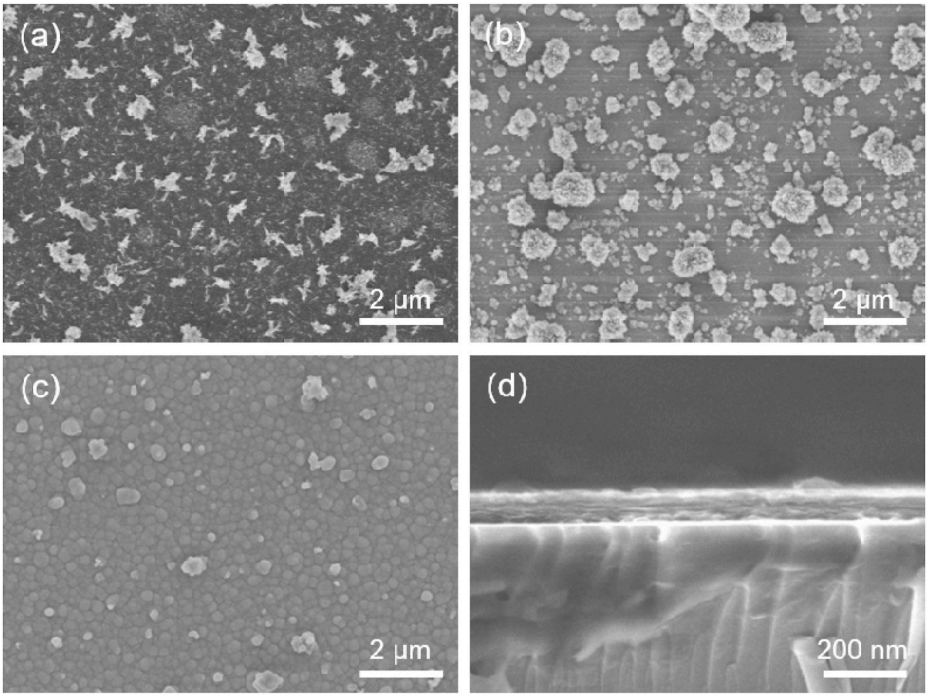

Fig. 2. Surface SEM images of single-layered ACOF-1 nanofilms generated by the first growth with different TFB concentrations. TFB concentrations of (a) 1.2 mM, (b) 2.4 mM and (c) 4.8 mM. Cross-sectional SEM image of ACOF-1 nanofilms with TFB concentration of 4.8 mM (d).

ACOF-1 nanofilm exhibits a continuous morphology with many grain boundaries among neighbouring nanocrystal domains, and the thickness is about ~120 nm (Fig. 2d).

The resulting first layer of ACOF-1 supported by silicon wafers were then subjected to secondary growth under a solvothermal environment to form the second layer of nanofilm that can offset against first layer at the interface, thus effectively narrowing the sieving size. We firstly studied the effect of TFB concentrations on the secondary growth of ACOF-1 nanofilms with a reaction duration of 24 h. ACOF-1 microcrystals continue to grow into larger domains and begin to merge with each other by further rising TFB concentrations (Fig. S4). At lower TFB concentration of 1.2 mM, a defective layer cannot completely cover first layer due to the little amount of COF microcrystals formed under this condition. (Fig. 3a and b). ACOF-1 microcrystals begin to merge with each other by further increasing the TFB concentration to 2.4 mM (Fig. S4a). More COF microcrystals grow into larger COF domains when TFB concentration increases to 4.8 mM. The surface morphology of ACOF-1 nanofilms shows no visible grain boundary and continuous, defect-free bi-layered nanofilms are formed (Fig. 3c). As TFB concentrations increase from 9.6 mM to 14.4 mM, the surface morphology of ACOF-1 nanofilms barely displays obvious change. Undoubtedly, we can speculate that discontinuous second layer leads to partly interlaced pores at the interface of first layer and second layer, while a defect-free second layer can promote a complete offset stacking at the interface to narrow the effective sieving size after secondary growth (Fig. 3d–f). In this work, the surface of bi-layered ACOF-1 nanofilms exhibits a morphology of intergrown COF domains self-assembled from many microcrystals (Figs. S6 and S8c), which could be attributed to Ostwald Ripening mechanism [38]. When TFB concentrations increase from 1.2 mM to 2.4 mM, the thicknesses of bi-layered ACOF-1 nanofilms maintain a slight increase from ~124 nm to ~137 nm (Figs. S5a–b). As TFB concentration increases to 4.8 mM, the thickness is signifcantly improved to ~312 nm and the bi-layered ACOF-1 nanofilms display obvious laminar structures (Fig. 3g). However, no obvious bi-layered structures can be observed in SEM images, which may be due to the good compatibility of the two ACOF-1 layers. When TFB concentrations vary from 9.6 mM to 14.4 mM, the thicknesses only increase from ~433 nm to ~454 nm and more pronounced layered-stacking structures can be observed (Figs. S5c–d). The reason for the increase in bi-layered nanofilm thickness and the formation of layered-stacking structures is that the terminal amino and aldehyde groups of single-layered ACOF-1 nanofilms can produce many nucleation sites to promote the deposition and growth of more COF microcrystals along the direction inherited from the first layers under the increased TFB concentrations. Moreover, the observation from SEM characterizations is consistent with the results measured by spectroscopic ellipsometry (Fig. 3h). The water contact angles of bi-layered ACOF-1 nanofilms increase slightly from 60° to 83° with the increase of TFB concentrations (Fig. S7a). However, these variations are not significant, which could be attributed to decreased surface roughnesses (Fig. S8).

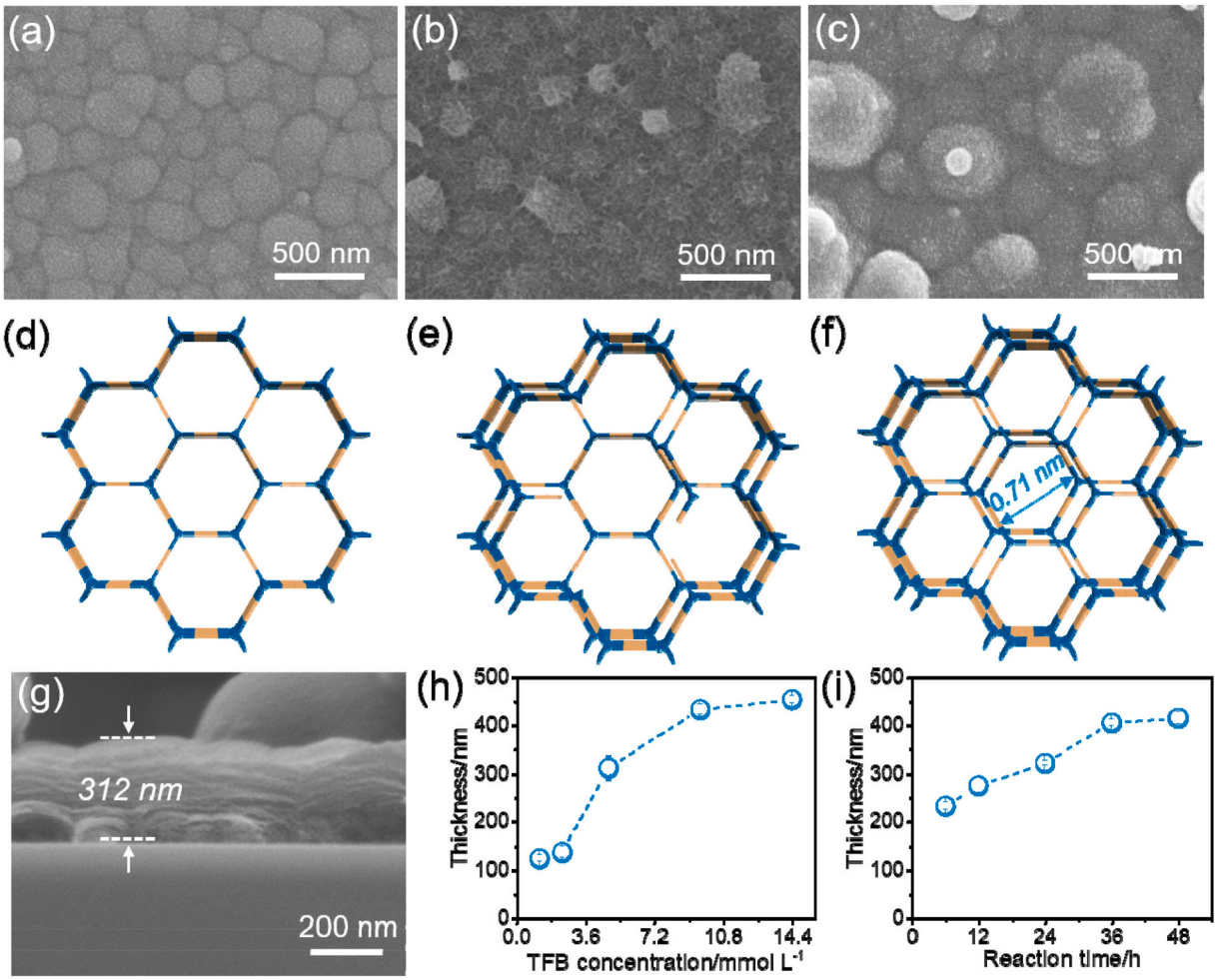

Fig. 3. Surface SEM images of bi-layered ACOF-1 nanofilms prepared via secondary growth with TFB concentrations of 0 mM (a), 1.2 mM (b) and 4.8 mM (c). Schematic diagram for the formation of bi-layered ACOF-1 nanofilms after secondary growth with increased TFB concentrations of 0 mM (d), 1.2 mM (e) and 4.8 mM (f). Cross-sectional SEM image of bi-layered ACOF-1 nanofilms prepared via secondary growth with the TFB concentration of 4.8 mM (g). Plot of the various thickness of bi-layered ACOF-1 nanofilms on different TFB concentrations (h) and reaction time (i) obtained by spectroscopic ellipsometry.

We also investigated the effect of reaction time on the secondary growth of single-layered ACOF-1 nanofilms with the TFB concentration of 4.8 mM. When the reaction time increases from 6 h to 48 h, the surface of bi-layered ACOF-1 nanofilms also shows a morphology of intergrown COF grains (Fig. S9). The bi-layered ACOF-1 nanofilms display obvious intercrystalline gaps grown at the reaction time of 6 h, which is too short to produce continuous layers (Fig. S9a). Rising the reaction time, which can promote the condensation between monomer pairs to provide more COF microcrystals for nanofilm growth, contributes to the formation of well intergrown COF grains in the absence of noticeable gaps, which is evidenced by the microscopic observations shown in Figs. S9b–e. Moreover, bi-layered ACOF-1 nanofilms still present layered-stacking structures, and the thickness increases gradually from ~232 nm to ~407 nm with prolonged reaction time from 6 h to 36 h, which is in accordance with results obtained by spectroscopic ellipsometry (Figs. 3i and S10). No further increase in the nanofilm thickness has been observed at long reaction time, such as 48 h, which could be caused by the complete consumption of monomers.

In short, increased TFB concentration can promote Schiff-based reaction, producing more COF microcrystals to prepare a batch of nanofilms with different microstructures and thicknesses. Reasonable reaction time may cause "self-healing" of COFs to enable high crystallization, and also accelerate the growth of ACOF-1 nanofilms. Therefore, TFB concentration and reaction time both exert an important influence on the growth of ACOF-1 nanofilms.

3.3. Separation performances of ACOF-1 composite membranes

Bi-layered ACOF-1 composite membranes were prepared through a perforated polymer-assisted transfer strategy reported in our previous work [29]. Particularly, the dense PSF-*b*-PEG layer coated on bi-layered ACOF-1 nanofilms was cavitated by following the mechanism of selective swelling-induced pore generation. It should be noted that PSF-*b*-PEG with robust PSF matrixes can offer an improved mechanical strength so as to realize the durability and stability of the protective layer, as well as good anti-fouling property duo to the hydrophilic PEG blocks [39,40]. As shown in Figs. S12a–b, the surface of PSF-*b*-PEG layer exhibits a perforated morphology composed of interconnected nanopores with a mean pore size of ~50 nm, and the entire thickness of the PSF-*b*-PEG layer is approximately 350 nm. With the assistance of PSF-*b*-PEG layers, we can easily and safely transfer the bi-layered ACOF-1 nanofilms from silicon wafers to water surface. Thus-obtained bi-layered ACOF-1 nanofilms are transparent (Figs. S12c–d), and the ACOF-1 membranes eventually display a tri-layered structure after compositing with macroporous PES supports, as shown in Fig. 4a and b. The bi-layered ACOF-1 nanofilm is closely adhered with the PES support, without any detachments or cracks, even after repeated bending and unfolding, which indicates a good interfacial stability (Fig. S13).

To confirm that bi-layered ACOF-1 nanofilms possess narrowed pore sizes after the secondary growth, we measured their separation performances to polyethylene glycols (PEGs) with different molecular weights. As shown in Fig. 4c, the rejection of the ACOF-1 composite membrane increases with rising PEG molecular weights, which is 38.8%, 85.5%, 93.6%, 95.9%, and 98.1%, respectively. Furthermore, the molecular weight cutoff (MWCO) of the ACOF-1 composite membrane is ~450 Da, which is defined as the molecular weight at the rejection rate of 90%. The pore radius distribution of bi-layered ACOF-1 nanofilms can be obtained through the following probability density function based on PEG rejection and Stokes radius (Fig. 4d) [41,42]. The mean pore radius of bi-layered ACOF-1 nanofilms is ~0.354 nm with a narrow pore radius distribution. Therefore, the bi-layered ACOF-1 nanofilms exhibits an effective sieving pore size of ~0.71 nm, which is smaller than the inherent pore width of ACOF-1 (~0.94 nm), demonstrating that the secondary growth to produce layer-by-layer nanofilms endows the thus-obtained bi-layered nanofilms with narrowed sieving pore sizes. The corresponding pore size distributions of ACOF-1 powders after first and secondary growth were further analyzed from nitrogen adsorption-desorption isotherms. As shown in Fig. S14, the effective pore size of ACOF-1 powders is constricted from ~0.9 nm to ~0.7 nm after secondary growth, which is consistent with the result calculated via PEG rejection and Stokes radius.

The ion separation performances of ACOF-1 composite membranes were then systematically explored, and we carried out filtration tests with various inorganic salt solutions as the feed. The pure PSF-*b*-PEG

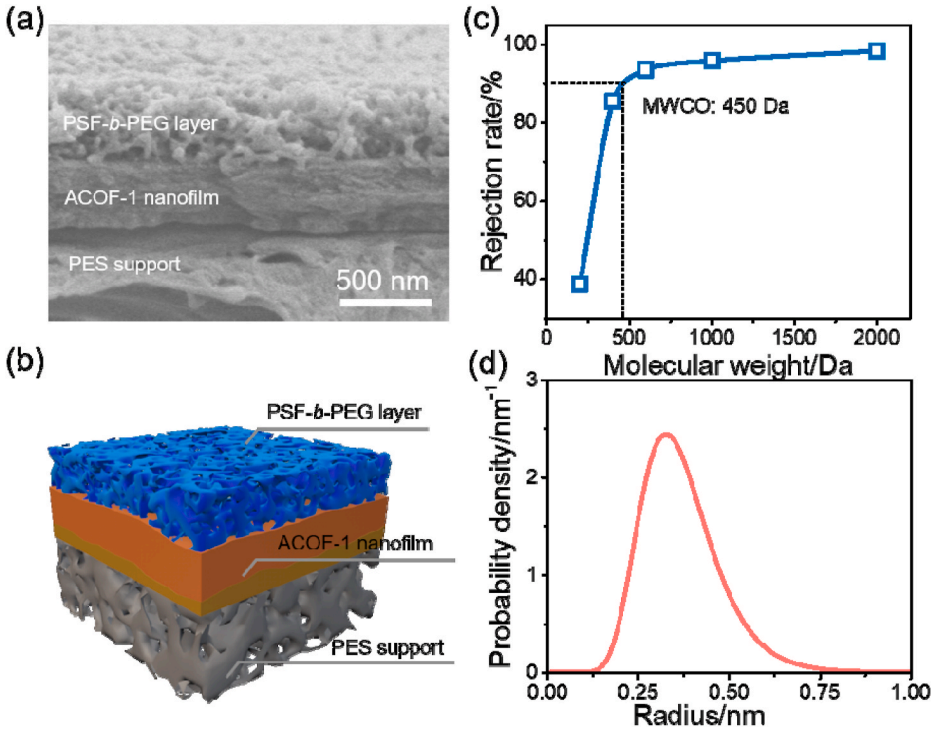

Fig. 4. (a) Cross-sectional SEM image of ACOF-1 composite membrane. (b) Schematic illustration of ACOF-1 composite membrane. (c) Rejection curve of the ACOF-1 composite membranes for PEG with various molecular weights. (d) The pore radius distribution of bi-layered ACOF-1 nanofilms calculated based on the rejection curve and a probability density function. The bi-layered ACOF-1 nanofilms prepared via secondary growth with TFB concentration of 4.8 mM and reaction time of 24 h.

layer exhibited a pure water permeance of ~2100 L m^{-2} h^{-1}. Here, the separation performance of the ACOF-1 composite membranes was preliminarily evaluated with a Na_2SO_4 aqueous solution. The single-layered ACOF-1 composite membrane subjected to the first growth gives a high flux ~50.1 L m^{-2} h^{-1} yet a negligible rejection of only ~6% toward Na_2SO_4. The poor desalination separation performance is probably because the inherent pore size of ACOF-1 is larger than the hydration diameter of salt ions, which inevitably results in a low ion selectivity. As shown in Fig. 5a and b, the second growth under various conditions always leads to a moderate decrease in flux but realizes a great improvement in rejection as expected. The influence of TFB concentrations during the second growth was first investigated with results given in Fig. 5a. Clearly, the concentrations significantly determine the desalination performance, as the rejection is enhanced from ~20.9% to 97.3% with increasing TFB concentrations from 1.2 mM to 14.4 mM. Under low TFB concentrations of 1.2 mM and 2.4 mM, bi-layered ACOF-1 composite membranes show a flux of ~14.2 L m^{-2} h^{-1} and ~5.6 L m^{-2} h^{-1} with relatively poor Na_2SO_4 rejection of ~20.9% and ~25.8% respectively, which is due to the incomplete coverage of COF microcrystals on the surface of single-layered ACOF-1nanofilms (Figs. 3b and S3a). Additionally, the flux of bi-layered ACOF-1 composite membranes prepared at TFB concentration of 4.8 mM declines to ~1.7 L m^{-2} h^{-1}, and the rejection sharply increases to ~95.7%. This result is probably because that the membrane thickness significantly increases and the offset channels form at the interface of nanofilms produced from the first and secondary growth (Fig. 3c). When TFB concentrations increased from 9.6 mM to 14.4 mM, the flux of bi-layered ACOF-1 composite membranes slightly decreases from ~1.3 L m^{-2} h^{-1} to ~1.1 L m^{-2} h^{-1} but the corresponding rejection exhibits no obvious increase, which is attributed to a slight variation in membrane thickness (Figs. S5c–d). Generally, the prepared bi-layered ACOF-1 composite membranes show better flux and higher rejection rate to a Na_2SO_4 solution at TFB concentration of 4.8 mM, which was selected to further study the secondary growth of bi-layered ACOF-1 nanofilms at different reaction time.

As shown in Fig. 5b, bi-layered ACOF-1 composite membranes with increased reaction time exhibit a very similar separation profile to membranes based on TFB concentrations. The flux of bi-layered ACOF-1 composite membranes reduces gradually from ~5.0 L m^{-2} h^{-1} to ~1.5 L m^{-2} h^{-1} with the increase of reaction time. At short reaction time of 6 h, bi-layered ACOF-1 composite membranes give a flux of ~5.0 L m^{-2} h^{-1} and Na_2SO_4 rejection of ~54.0%. With increased reaction time to 12 h, the bi-layered ACOF-1 composite membrane shows a flux of ~2.1 L m^{-2} h^{-1} and Na_2SO_4 rejection of ~82.9%, which is ascribed to highly compact surface coverage with COF microcrystals on the first layer and increased membrane thickness. Obviously, the flux of bi-layered ACOF-1 composite membrane prepared at 24 h declines to ~1.7 L m^{-2} h^{-1} but Na_2SO_4 rejection is up to ~95.7% considering a reduced effective aperture. As the reaction time increases to 36 h and 48 h, the separation performance of bi-layered ACOF-1 composite membranes shows little variation.

Considering that the rejection rates of ACOF-1 nanofilms show a very similar variation profile to the thicknesses under different conditions (Fig. 3h and i), one may argue that the increase in rejection rates could possibly originate from the elevated thicknesses. In this case, we also prepared the thick single-layered ACOF-1 nanofilms with the thickness of up to ~300 nm by the first growth under an enhanced growth condition (Fig. S13). Compared with obtained bi-layered nanofilms, thus-synthesized thick ACOF-1 nanofilms show a flux of ~5.7 L m^{-2} h^{-1} with a humble Na_2SO_4 rejection of ~11.9%, indicating that the increased rejection rates of ACOF-1 nanofilms mainly depend on the narrowed pore sizes instead of increased thicknesses. Among all the bi-layered ACOF-1 composite membranes, the membrane prepared with TFB concentration of 4.8 mM and reaction time of 24 h exhibits the best performance in consideration of both the flux and rejection to Na_2SO_4. We therefore choose this membrane to examine the separation performance towards various salt solutions in detail, including Na_2SO_4, $MgSO_4$, $MgCl_2$, and NaCl. As shown in Fig. 5c, the rejection rates of the bi-layered ACOF-1 composite membrane to Na_2SO_4, $MgSO_4$, $MgCl_2$, and NaCl are 95.7%, 90.2%, 69.6%, and 43.0% respectively, and follow the order of Na_2SO_4 > $MgSO_4$ > $MgCl_2$ > NaCl. The bi-layered ACOF-1 composite membrane presents high rejection rates toward divalent ions and moderate rejection rates for monovalent ions, which originates from larger hydration radius of divalent ions than monovalent ions, making them difficult to permeate through the bi-layered ACOF-1 nanofilms

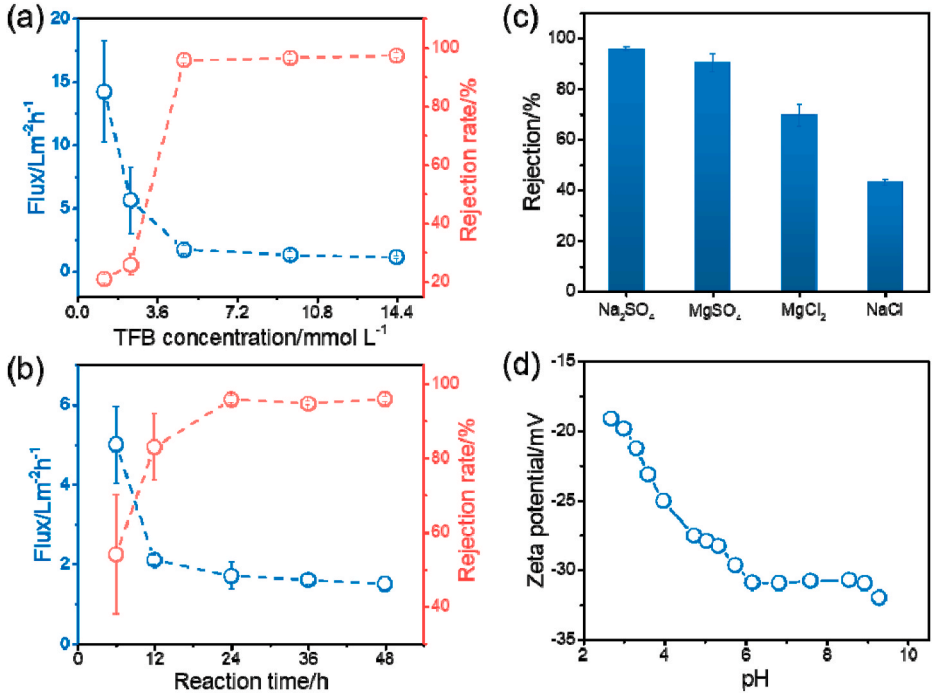

Fig. 5. Flux and rejection of ACOF-1 composite membranes prepared with different TFB concentrations (a) and reaction time (b). Rejection of ACOF-1 composite membranes toward different salt solutions under the optimal synthetic condition (c). Zeta potentials of bi-layered ACOF-1 nanofilms after secondary growth (d).

[43]. Moreover, the bi-layered COF nanofilms are negatively charged according to Fig. 5d, they usually behave higher rejection to Na_2SO_4 than $MgSO_4$ under the synergistic effect of both size sieving and Donann effect, which is because that the charged groups on the membrane easily attract the Mg^{2+} over Na^+ [44]. The desired separation performances of ACOF-1 composite membranes produced by continuously filtrating inorganic salt solution for a long period duration of 24 h reveal a good long-term stability of our membranes as well. Compared with other COF membranes reported in literatures (Table S1), the bi-layered ACOF-1 composite membrane shows a reasonable flux with a satisfying rejection rate to Na_2SO_4, and we believe that elaborately designed COF membranes will shine for desalination in the future.

4. Conclusions

In summary, we have successfully prepared bi-layered ACOF-1 nanofilms for desalination by the secondary growth. ACOF-1 microcrystals grow to form well-intergrown bi-layered ACOF-1 nanofilms, which have conspicuous layered structures and well-tunable thicknesses at a nanometer scale depending on the precursor concentrations and reaction durations. The secondary growth not only imposes better control over the microstructure and thickness of bi-layered ACOF-1 nanofilms, but also narrows the sieving pore size, resulting in significantly improved desalination performances. After optimizing the synthesis condition, the bi-layered ACOF composite membrane exhibits a reasonable flux and a high Na_2SO_4 rejection rate of ~95.7%. This work is expected to facilitate the development of COF-based membranes with subnanometer channels for desalination and precise molecular separations. Moreover, similar benefits may be acquired by applying this methodology to other framework-based materials.

Author statement

Ankang Xiao: Investigation, Methodology, Writing-Original Draft.
Xiansong Shi: Investigation, Writing-Review & Editing.
Zhe Zhang: Investigation.
Congcong Yin: Investigation.
Sen Xiong: Investigation, Funding acquisition.
Yong Wang: Supervision, Writing-Review & Editing, Funding acquisition.

Declaration of competing interest

The authors declare that they have no known competing financial interests or personal relationships that could have appeared to influence the work reported in this paper.

Acknowledgements

Financial supports from the National Science Foundation of China (21825803, 21908096) and Jiangsu Natural Science Foundation (BK20190677) are acknowledged.

Appendix A. Supplementary data

Supplementary data to this article can be found online at https://doi.org/10.1016/j.memsci.2021.119122.

References

[1] A.P. Côté, A.I. Benin, N.W. Ockwig, M. O'Keeffe, A.J. Matzger, O.M. Yaghi, Porous, crystalline, covalent organic frameworks, Science 310 (2005) 1166–1170.
[2] X. Feng, X. Ding, D. Jiang, Covalent organic frameworks, Chem. Soc. Rev. 41 (2012) 6010–6022.
[3] C.J. Doonan, D.J. Tranchemontagne, T.G. Glover, J.R. Hunt, O.M. Yaghi, Exceptional ammonia uptake by a covalent organic framework, Nat. Chem. 2 (2010) 235–238.
[4] H. Furukawa, O.M. Yaghi, Storage of hydrogen, methane, and carbon dioxide in highly porous covalent organic frameworks for clean energy applications, J. Am. Chem. Soc. 131 (2009) 8875–8883.
[5] J. Thote, H.B. Aiyappa, A. Deshpande, D. Diaz Diaz, S. Kurungot, R. Banerjee, A covalent organic framework-cadmium sulfide hybrid as a prototype photocatalyst for visible-light-driven hydrogen production, Chemistry 20 (2014) 15961–15965.
[6] S. Lin, C.S. Diercks, Y. Zhang, N. Kornienko, E.M. Nichols, Y. Zhao, A.R. Paris, D. Kim, P. Yang, O.M. Yaghi, C.J. Chang, Covalent organic frameworks comprising cobalt porphyrins for catalytic CO_2 reduction in water, Science 349 (2015) 1208–1213.
[7] M. Calik, F. Auras, L.M. Salonen, K. Bader, I. Grill, M. Handloser, D.D. Medina, M. Dogru, F. Lobermann, D. Trauner, A. Hartschuh, T. Bein, Extraction of photogenerated electrons and holes from a covalent organic framework integrated heterojunction, J. Am. Chem. Soc. 136 (2014) 17802–17807.
[8] L. Chen, K. Furukawa, J. Gao, A. Nagai, T. Nakamura, Y. Dong, D. Jiang, Photoelectric covalent organic frameworks: converting open lattices into ordered donor-acceptor heterojunctions, J. Am. Chem. Soc. 136 (2014) 9806–9809.
[9] J. Li, X. Zhou, J. Wang, X. Li, Two-dimensional covalent organic frameworks (COFs) for membrane separation: a mini review, Ind. Eng. Chem. Res. 58 (2019) 15394–15406.
[10] C. Zhang, B.H. Wu, M.Q. Ma, Z. Wang, Z.K. Xu, Ultrathin metal/covalent-organic framework membranes towards ultimate separation, Chem. Soc. Rev. 48 (2019) 3811–3841.
[11] M.A. Khayum, V. Vijayakumar, S. Karak, S. Kandambeth, M. Bhadra, K. Suresh, N. Acharambath, S. Kurungot, R. Banerjee, Convergent covalent organic framework thin sheets as flexible supercapacitor electrodes, ACS Appl. Mater. Interfaces 10 (2018) 28139–28146.
[12] T. Sick, A.G. Hufnagel, J. Kampmann, I. Kondofersky, M. Calik, J.M. Rotter, A. Evans, M. Doblinger, S. Herbert, K. Peters, D. Bohm, P. Knochel, D.D. Medina, D. Fattakhova-Rohlfing, T. Bein, Oriented films of conjugated 2D covalent organic frameworks as photocathodes for water splitting, J. Am. Chem. Soc. 140 (2018) 2085–2092.
[13] D.B. Shinde, G. Sheng, X. Li, M. Ostwal, A.H. Emwas, K.W. Huang, Z. Lai, Crystalline 2D covalent organic framework membranes for high-flux organic solvent nanofiltration, J. Am. Chem. Soc. 140 (2018) 14342–14349.
[14] F. Pan, W. Guo, Y. Su, N.A. Khan, H. Yang, Z. Jiang, Direct growth of covalent organic framework nanofiltration membranes on modified porous substrates for dyes separation, Separ. Purif. Technol. 215 (2019) 582–589.
[15] H. Fan, A. Mundstock, J. Gu, H. Meng, J. Caro, An azine-linked covalent organic framework ACOF-1 membrane for highly selective CO_2/CH_4 separation, J. Mater. Chem. A 6 (2018) 16849–16853.
[16] H. Fan, M. Peng, I. Strauss, A. Mundstock, H. Meng, J. Caro, High-flux vertically aligned 2D covalent organic framework membrane with enhanced hydrogen separation, J. Am. Chem. Soc. 142 (2020) 6872–6877.
[17] K. Dey, M. Pal, K.C. Rout, H.S. Kunjattu, A. Das, R. Mukherjee, U.K. Kharul, R. Banerjee, Selective molecular separation by interfacially crystallized covalent organic framework thin films, J. Am. Chem. Soc. 139 (2017) 13083–13091.
[18] R. Wang, X. Shi, A. Xiao, W. Zhou, Y. Wang, Interfacial polymerization of covalent organic frameworks (COFs) on polymeric substrates for molecular separations, J. Membr. Sci. 566 (2018) 197–204.
[19] W. Zhang, L. Zhang, H. Zhao, B. Li, H. Ma, A two-dimensional cationic covalent organic framework membrane for selective molecular sieving, J. Mater. Chem. A 6 (2018) 13331–13339.
[20] G. Li, K. Zhang, T. Tsuru, Two-dimensional covalent organic framework (COF) membranes fabricated via the assembly of exfoliated COF nanosheets, ACS Appl. Mater. Interfaces 9 (2017) 8433–8436.
[21] C. Yin, Z. Zhang, J. Zhou, Y. Wang, Single-layered nanosheets of covalent triazine frameworks (CTFs) by mild oxidation for molecular-sieving membranes, ACS Appl. Mater. Interfaces 12 (2020) 18944–18951.
[22] X. Shi, D. Ma, F. Xu, Z. Zhang, Y. Wang, Table-salt enabled interface-confined synthesis of covalent organic framework (COF) nanosheets, Chem. Sci. 11 (2020) 989–996.
[23] D. Hao, J. Zhang, H. Lu, W. Leng, R. Ge, X. Dai, Y. Gao, Fabrication of a COF-5 membrane on a functionalized α-Al_2O_3 ceramic support using a microwave irradiation method, Chem. Commun. 50 (2014) 1462–1464.
[24] S. Hao, L. Jiang, Y. Li, Z. Jia, B. Van der Bruggen, Facile preparation of COF composite membranes for nanofiltration by stoichiometric spraying layer-by-layer self-assembly, Chem. Commun. 56 (2020) 419–422.
[25] N.A. Khan, R. Zhang, H. Wu, J. Shen, J. Yuan, C. Fan, L. Cao, M.A. Olson, Z. Jiang, Solid-vapor interface engineered covalent organic framework membranes for molecular separation, J. Am. Chem. Soc. 142 (2020) 13450–13458.
[26] S. Kandambeth, B.P. Biswal, H.D. Chaudhari, K.C. Rout, H.S. Kunjattu, S. Mitra, S. Karak, A. Das, R. Mukherjee, U.K. Kharul, R. Banerjee, Selective molecular sieving in self-standing porous covalent-organic-framework membranes, Adv. Mater. 29 (2017) 1603945.
[27] H. Fan, J. Gu, H. Meng, A. Knebel, J. Caro, High-flux membranes based on the covalent organic framework COF-LZU1 for selective dye separation by nanofiltration, Angew. Chem. Int. Ed. 57 (2018) 4083–4087.
[28] X. Shi, A. Xiao, C. Zhang, Y. Wang, Growing covalent organic frameworks on porous substrates for molecule-sieving membranes with pores tunable from ultra- to nanofiltration, J. Membr. Sci. 576 (2019) 116–122.
[29] A. Xiao, Z. Zhang, X. Shi, Y. Wang, Enabling covalent organic framework nanofilms for molecular separation: perforated polymer-assisted transfer, ACS Appl. Mater. Interfaces 11 (2019) 44783–44791.

[30] K. Geng, T. He, R. Liu, S. Dalapati, K.T. Tan, Z. Li, S. Tao, Y. Gong, Q. Jiang, D. Jiang, Covalent organic frameworks: design, synthesis, and functions, Chem. Rev. 120 (2020) 8814–8933.
[31] C. Liu, Y. Jiang, A. Nalaparaju, J. Jiang, A. Huang, Post-synthesis of a covalent organic framework nanofiltration membrane for highly efficient water treatment, J. Mater. Chem. A 7 (2019) 24205–24210.
[32] Y. Li, Q. Wu, X. Guo, M. Zhang, B. Chen, G. Wei, X. Li, X. Li, S. Li, L. Ma, Laminated self-standing covalent organic framework membrane with uniformly distributed subnanopores for ionic and molecular sieving, Nat. Commun. 11 (2020) 599.
[33] W. Zhou, M. Wei, X. Zhang, F. Xu, Y. Wang, Fast desalination by multilayered covalent organic framework (COF) nanosheets, ACS Appl. Mater. Interfaces 11 (2019) 16847–16854.
[34] H. Fan, A. Mundstock, A. Feldhoff, A. Knebel, J. Gu, H. Meng, J. Caro, Covalent organic framework-covalent organic framework bilayer membranes for highly selective gas separation, J. Am. Chem. Soc. 140 (2018) 10094–10098.
[35] L. Gui, J. Dong, W. Fang, S. Zhang, K. Zhou, Y. Zhu, Y. Zhang, J. Jin, Ultrafast ion sieving from honeycomb-like polyamide membranes formed using porous protein assemblies, Nano Lett. 20 (2020) 5821–5829.
[36] Z. Li, X. Feng, Y. Zou, Y. Zhang, H. Xia, X. Liu, Y. Mu, A 2D azine-linked covalent organic framework for gas storage applications, Chem. Commun. 50 (2014) 13825–13828.
[37] L. Stegbauer, M.W. Hahn, A. Jentys, G. Savasci, C. Ochsenfeld, J.A. Lercher, B. V. Lotsch, Tunable water and CO_2 sorption properties in isostructural azine-based covalent organic frameworks through polarity engineering, Chem. Mater. 27 (2015) 7874–7881.
[38] S. Kandambeth, V. Venkatesh, D.B. Shinde, S. Kumari, A. Halder, S. Verma, R. Banerjee, Self-templated chemically stable hollow spherical covalent organic framework, Nat. Commun. 6 (2015) 6786.
[39] D. Zhong, Z. Wang, Q. Lan, Y. Wang, Selective swelling of block copolymer ultrafiltration membranes for enhanced water permeability and fouling resistance, J. Membr. Sci. 558 (2018) 106–112.
[40] N. Wang, T. Wang, Y. Hu, Tailoring membrane surface properties and ultrafiltration performances via the self-assembly of polyethylene glycol-block-polysulfone-block-polyethylene glycol block copolymer upon thermal and solvent annealing, ACS Appl. Mater. Interfaces 9 (2017) 31018–31030.
[41] S. Gao, Y. Zhu, Y. Gong, Z. Wang, W. Fang, J. Jin, Ultrathin polyamide nanofiltration membrane fabricated on brush-painted single-walled carbon nanotube network support for ion sieving, ACS Nano 13 (2019) 5278–5290.
[42] J. Lin, W. Ye, M.-C. Baltaru, Y.P. Tang, N.J. Bernstein, P. Gao, S. Balta, M. Vlad, A. Volodin, A. Sotto, P. Luis, A.L. Zydney, B. Van der Bruggen, Tight ultrafiltration membranes for enhanced separation of dyes and Na_2SO_4 during textile wastewater treatment, J. Membr. Sci. 514 (2016) 217–228.
[43] R. Wang, M. Wei, Y. Wang, Secondary growth of covalent organic frameworks (COFs) on porous substrates for fast desalination, J. Membr. Sci. 604 (2020) 118090.
[44] X. Zhang, Y. Lv, H.-C. Yang, Y. Du, Z.-K. Xu, Polyphenol coating as an interlayer for thin-film composite membranes with enhanced nanofiltration performance, ACS Appl. Mater. Interfaces 8 (2016) 32512–32519.